

Research Article



Rare-Earth Separation Very Important Paper

How to cite: Angew. Chem. Int. Ed. 2024, 63, e202410233 doi.org/10.1002/anie.202410233

Chelator-Assisted Precipitation-Based Separation of the Rare Earth Elements Neodymium and Dysprosium from Aqueous Solutions

Yangyang Gao, Gerra L. Licup, Nicholas P. Bigham, David C. Cantu,* and Justin J. Wilson*

Abstract: The rare earth elements (REEs) are critical resources for many clean energy technologies, but are difficult to obtain in their elementally pure forms because of their nearly identical chemical properties. Here, an analogue of macropa, G-macropa, was synthesized and employed for an aqueous precipitation-based separation of Nd³⁺ and Dy³⁺. G-macropa maintains the same thermodynamic preference for the large REEs as macropa, but shows smaller thermodynamic stability constants. Molecular dynamics studies demonstrate that the binding affinity differences of these chelators for Nd3+ and Dy3+ is a consequence of the presence or absence of an inner-sphere water molecule, which alters the donor strength of the macrocyclic ethers. Leveraging the small REE affinity of G-macropa, we demonstrate that within aqueous solutions of Nd3+, Dy3+, and Gmacropa, the addition of HCO₃⁻ selectively precipitates Dy₂(CO₃)₃, leaving the Nd³⁺-G-macropa complex in solution. With this method, remarkably high separation factors of 841 and 741 are achieved for 50:50 and 75:25 mixtures. Further studies involving Nd³⁺:Dy³⁺ ratios of 95:5 in authentic magnet waste also afford an efficient separation as well. Lastly, G-macropa is recovered via crystallization with HCl and used for subsequent extractions, demonstrating its good recyclability.

Introduction

In 2010, terbium (Tb), dysprosium (Dy), europium (Eu), neodymium (Nd), and yttrium (Y) were identified to be the most essential rare earth elements (REEs) by the U.S. Department of Energy because of their critical applications

[*] Y. Gao, N. P. Bigham, J. J. Wilson Department of Chemistry and Chemical Biology Cornell University Ithaca, New York 14853, United States

Y. Gao, J. J. Wilson Department of Chemistry and Biochemistry University of California, Santa Barbara Santa Barbara, California 93106, United States E-mail: justinjwilson@ucsb.edu

G. L. Licup, D. C. Cantu Department of Chemical and Materials Engineering University of Nevada, Reno Reno, Nevada 89557, United States E-mail: dcantu@unr.edu

for clean energy technologies. [1-4] Even within China, the largest international REE supplier, the reserves of middle and heavy REEs are estimated to last less than 20 years at current mining rates.^[5-7] The limited availability and technological necessity of these valuable REEs have spurred a number of innovative efforts to recycle and reuse them from secondary sources, including manufacturing waste and spent materials.[8-12] Among these five REEs, Nd and Dy are often intimately combined in Nd₂Fe₁₄B permanent magnets. These magnets contain up to 30 wt % Nd with smaller quantities of Dy as an additive, providing a valuable resource for these critical elements.[10,13] Similarly, other electronic waste and optical components contain Nd and Dy, albeit in lower amounts.[14,15] The ability to effectively extract and subsequently separate Nd and Dy would be an important contribution towards addressing the REE supply crisis. [16]

The chemical similarity of these REEs, however, has led challenges for developing efficient separation strategies.[4,17] The only significant difference is their ionic radii, which contracts across the series.[18-21] The current separation approach employed industrially is solvent extraction, [22-25] where an organic solvent, like kerosene, containing extractant, such bis(2ethylhexyl)phosphoric acid (HDEHP, Figure 1), is contacted with a lanthanide- (Ln3+)-containing aqueous solution. [26,27] The different ionic radii gives them a slight difference in affinity for HDEHP, leading to a minimally selective extraction of smaller REEs into the organic phase. Due to the low efficiency of this process, multiple extraction stages are required to achieve suitably pure REEs. [23,25] The introduction of a ligand in the aqueous phase can improve these separations. For example, a water-soluble bis-lactam-1,10-phenanthroline (aqBLPhen, Figure 1) coupled with an oil-soluble diglycolamide extractant could separate Nd3+ and Dy3+ with suitable efficiency. [28] A concern in solvent extraction techniques, however, is the generation of large amounts of liquid waste, which contributes to the environmental burden of REE separation. [29-31] Furthermore, the toxicity of phosphorus-based extractants and organic solvents is problematic for both humans and aquatic organisms. [32-34] Therefore, more efficient and environmentally benign separation strategies are needed.

As one alternative approach, solid-phase separations have been developed using solid adsorbents that contain metal-binding groups to capture ions from solution. [35-39] This strategy minimizes organic solvent use, and the solid adsorbents can be regenerated with different stripping eluents. For example, XAD-7 resin impregnated with di(2ethylhexyl) phosphoric acid (D2EHPA) can efficiently





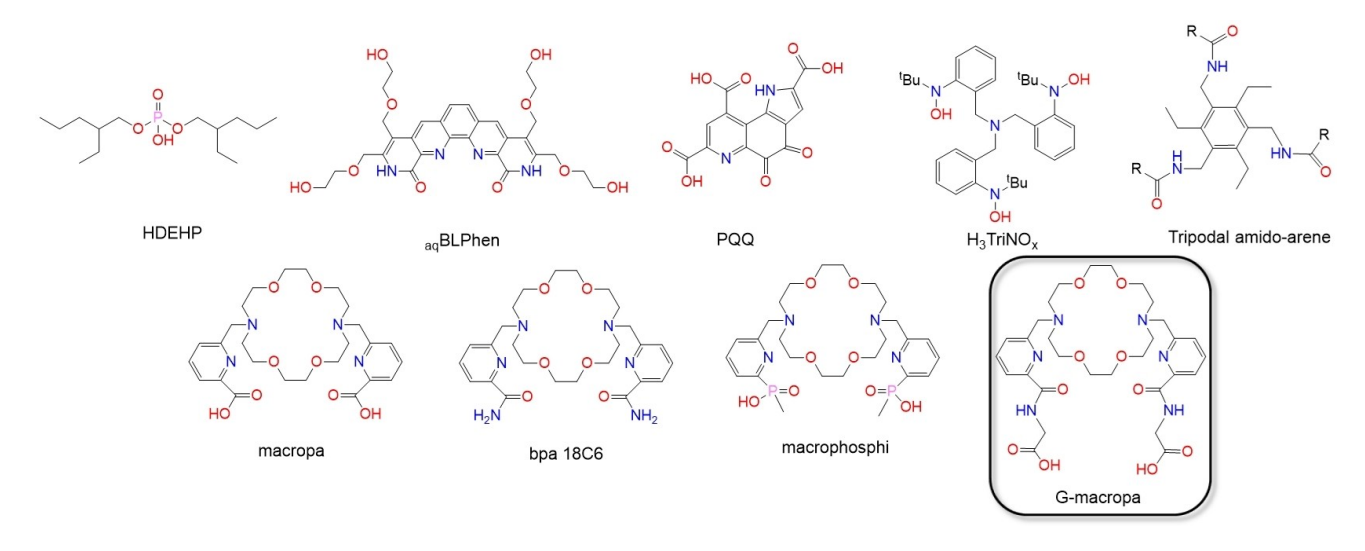


Figure 1. Chemical structures of the ligands discussed in this work. The R group in the tripodal amido-arene ligand is $-C_8H_{17}$.

extract light REEs, [40] and biological ligands, like lanmodulin and its variants, adsorbed to agarose, can extract and separate of Dy³+ and Nd³+.[41-44] Solid-phase extraction, however, still requires the development and characterization of new solid adsorbents.

Selective precipitation would be another important advance due to its relative simplicity, low-energy input, and good economic feasibility. [45-49] Within the REE series, however, the solubility difference of these ions with typical counterions, like oxalate and carbonate, is not sufficient for good separations.^[50-52] Researchers have explored the different chelators to enhance the solubility differences of REE complexes.^[47,53-55] For example, a tripodal ligand, TriNOx³⁻ (Figure 1) can selectively precipitate Dy³⁺ from a benzene solution also containing Nd3+, achieving a separation factor (SF) of 359. [56] Leveraging the different magnetic properties of REEs, this chelator was also used to selectively crystallize heavy REEs in an external magnetic field, achieving an SF of 494 for La/Dy separation.^[57] The methanol dehydrogenase cofactor, pyrroloquinoline quinone (PQQ, Figure 1), can also selectively precipitate the light REEs (Ce-Eu) from the heavy REEs. [58] A tripodal amido-arene ligand (Figure 1) can selectively precipitate light REE nitratometalates as supramolecular capsules at a toluene/HNO3 interface. [59] In addition to solubility modulation, REEs can also be selectively incorporated into solid-state materials.^[60-64] For example, synthesis of lanthanide borate yields different structural types that allowed for floatation-based separation of Nd and Dy (SF 986). [65] These innovative REE precipitation strategies highlight how the implementation of chelators and appropriate anions can accomplish selective separation. Despite the promise of these systems, they have several disadvantages. For example, some of these systems requires high temperatures or organic solvents that limit their large-scale application. As such, developing operationally simple precipitation-based REE separations in aqueous solution is highly desired.

We and others have worked extensively with water-soluble chelators based on the diaza-18-crown-6 macrocycle. [66-71] These ligands exhibit a reverse-size selectivity, stronger binding to the light over heavy lanthanides. In particular, macropa (Figure 1) has been applied in nuclear medicine applications and actinide separation. Subsequent modifications to the pendent donor arms have afforded chelators maintain this reverse-size selectivity but show different thermodynamic trends. For example, macrophosphi (Figure 1), with pendent phosphinate donors, exhibits a different binding preference for the light REEs compared to macropa, [69] enabling effective separation of adjacent La³⁺ and Ce³⁺ via liquid extraction.

In this work, we developed a glycine conjugate of macropa, called G-macropa, for a straightforward precipitation-based separation of REEs. G-macropa can stabilize the light REEs in aqueous solution, while allowing the heavy REEs to be precipitated by carbonate. Macropa fails for this application because its binding affinity for heavy REEs is too strong to enable facile precipitation with counterions. We reasoned that the neutral picolinamide donors would form lower-stability REEs complexes, and the glycine moieties would enhance its water solubility, [72,73] features that were noted for the corresponding glycine an analogue of DOTA. Using this approach, we obtained analytically pure Dy₂(CO₃)₃ from aqueous solutions of Nd³⁺ and Dy³⁺ in different ratios, demonstrating a promising and environmentally friendly approach for isolating these critical minerals. Overall, this work shows that amplifying the subtle coordination differences of the Ln3+ with water-soluble chelators, can give efficient REE separation in aqueous solutions.



Scheme 1. Synthesis of G-macropa.

Results and Discussion

G-macropa: Synthesis, and Characterization

G-macropa was synthesized from macropa via amide coupling, followed by ester deprotection under basic conditions, and the conversion to free acid form with 6 M HCl (Scheme 1). G-macropa and its synthetic intermediates were fully characterized by NMR spectroscopy, electrospray ionization high-resolution mass spectrometry (ESI-HRMS), elemental analysis, and high-performance liquid chromatography (HPLC) (Figures S1-S8). The solid-state structure of protonated G-macropa was determined by X-ray crystallography (Figure 2 and Table S1). G-macropa crystallizes in the triclinic $P\overline{1}$ space group with the centroid of the macrocycle residing on a crystallographic inversion center. Given the acidic crystallization conditions, the terminal carboxylic acids, as well as the tertiary amines within the macrocyclic core, are protonated, as verified by the location of electron density on the difference Fourier map and the presence of hydrogen-bonding interactions within the crystal lattice (Figure S9).

Solution Characterization of Ln3+ Complexes of G-macropa

The coordination chemistry of G-macropa with the REEs was investigated with NMR and UV/Vis spectroscopy. The largest and smallest diamagnetic REE La³⁺ and Lu³⁺ were used in these studies. The ¹H, ¹³C{¹H} and 2D (COSY and HMBC) NMR spectra (pD 7, D₂O), as well as the ESI-

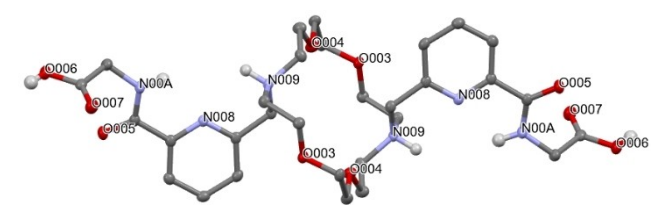


Figure 2. Crystal structure of H_2G -macropa²⁺. For clarity, hydrogen atoms attached to carbon centers are omitted. Thermal displacement ellipsoids are drawn at the 50% probability.

HRMS data of a 1:1 mixture of La³⁺ and G-macropa give characteristic features signifying the formation of the [La(Gmacropa)]+ (Figures S10-14). For example, the ¹H NMR spectrum shows diastereotopic splitting of the methylene CH₂ resonances of the picolinamide arms, a feature that signifies complex formation (Figure S10). [67,74] Furthermore, the ESI-HRMS reveals molecular ion peaks at m/z =261.733, 392.096, and 783.184, which agree well with the expected values for the $[M+2H]^{3+}$ (calcd. m/z=261.734), $[M+H]^{2+}$ (calcd. m/z=392.097), and $[M]^+$ (calcd. m/z=783.186) ions (Figure S14). Under identical conditions, a 1:1 mixture of Lu³⁺ and G-macropa does not afford any significant spectroscopic changes from the free ligand (Figures S15–17). Given the importance of Nd³⁺ and Dy³⁺ within electronic waste, we explored their macropa and Gmacropa complexes by ¹H NMR spectroscopy. Mixtures of Nd3+ and either macropa or G-macropa in a 1:1 molar ratio in pD 7 D₂O afford spectra displaying a range of paramagnetically shifted resonances spanning -15 to +15 ppm (Figure S18) without any signals arising from free diamagnetic macropa or G-macropa. Under identical conditions, a mixture of Dy³⁺ and macropa displays intense paramagnetically shifted resonances spanning -250 to +250 ppm (Figure S19). By contrast, the ¹H NMR spectrum of Dy³⁺ and G-macropa mixture primarily shows signals within the diamagnetic region, attributed to free ligand. Thus, these results demonstrate the G-macropa can bind to the larger Nd³⁺, but not the smaller Dy³⁺.

Thermodynamic Solution Studies

To further probe the effects of the pendent glycine residues on the REE-binding properties of G-macropa, the protonation constants (K_i) and the REE stability constants (K_{LnL}) were determined by potentiometric titration over a pH range of 2.5–11.3 (Figures S20–28). The protonation constants of macropa, bpa 18C6 (Figure 1), and macrophosphi, as well as their REE stability constants are provided in Table 1 for comparison. These constants, K_i and K_{LnL} , are defined below in Eqs 1 and 2, respectively, where L corresponds to the fully deprotonated chelator.

5213773, 2024, 42, Downloaded from https://onlinelibrary.wiley.com/doi/10.1002/anie.202410233 by University Of Nevada Reno, Wiley Online Library on [12/05/2025]. See the Terms and Conditions (https://onlinelibrary.wiley.com/terms-and-conditions) on Wiley Online Library for rules of use; OA articles are governed by the applicable Creative Commons. License

Table 1: Protonation constants of G-macropa and thermodynamic stability constants of its Ln^{3+} complexes determined by pH potentiometry (25 °C and I = 0.1 M KCl).

	G-macropa ²⁻	bpa 18C6	macrophosphi ²⁻	macropa ²⁻
log K _{a1}	7.86(3) ^[a]	7.08	8.13	7.41
$\log K_{a2}$	6.55(1) ^[a]	6.40	6.77	6.85
$log K_{a3}$	3.38(3) ^[a]		1.97	3.32
$\log K_{a4}$				2.36
$\log K_{a5}$				1.96
$\log K_{LaL}$	10.49(1) ^[a]	8.63	12.94	14.99
log KceL	9.89(4) ^[a]		11.92	15.11
$\log K_{Prl}$	9.06(2) ^[a]		11.12	14.70
log K _{NdL}	8.22(6) ^[a]		10.44	14.36
$\log K_{SmL}$	6.65(1) ^[a]		9.34	13.80
log K _{EuL}	6.05(2) ^[a]	5.17	8.68	13.01
$\log K_{GdL}$	5.50(5) ^[a]		7.82	13.02
$\log K_{TbL}$	5.01 (2) ^[a]		7.24	11.79
$\log K_{DyL}$			6.83	11.72
log K _{HoL}			6.69	10.59
$\log K_{ErL}$			6.73	10.10
$\log K_{TmL}$			6.76	9.95
$\log K_{YbL}$			6.78	8.89
$\log K_{LuL}$			6.67	8.25

[a] Values in parentheses are the standard deviations of the last significant Figures resulting from 7 independent measurements for protonation constant and 3 independent measurements for stability constant.

$$K_i = [H_i L]/[H^+] [H_{i-1} L]$$
 (1)

$$K_{LnL} = [LnL]/[Ln^{3+}] [L]$$
(2)

For G-macropa, four protonation constants could be determined within this pH range. The first two protonation constants ($\log K_{a1} = 7.86$ and $\log K_{a2} = 6.55$) are assigned to the successive protonation of the tertiary amine nitrogen atoms within the macrocycle. The third and fourth protonation constants ($\log K_{a3} = 3.38$ and $\log K_{a4} = 2.51$) are assigned to the carboxylic acid groups on the pendent glycine. Like bpa 18C6, [75] the K_i of the neutral pendent picolinamide donors cannot be measured within this pH range via potentiometry. The identical sum of the first two log K_i (14.41 and 14.26) of G-macropa and macropa, respectively, suggests that the conjugation of glycine does not alter the basicity of the macrocycle, but only that of the pendent donor arms. With these protonation constants in hand, we determined the log K_{LnL} values across the REE series with G-macropa and REE ions in a molar ratio of 1.0 to 0.95 (Table 1 and Figure 3). Under these conditions, the titration curves for the heavy REEs (Dy3+-Lu3+) were unchanged relative to the free ligands, until reaching pH > 5.3, where hydrolysis of Ln³⁺ occurs. Even the use of 3 equiv. of Gmacropa did not give any indication of metal binding. Thus, the log K_{LnL} of the heavy REEs are too low to be measured via pH potentiometric titration and are therefore less than 5. This result is consistent with the failed attempt to characterize the Lu^{3+} complex via NMR and UV/Vis spectroscopy. A higher affinity was found for the light REEs (log K_{LaL} = 10.49 versus log K_{TbL} =5.01), indicating that G-macropa retains the reverse-size selectivity of other diaza-18-crown-6

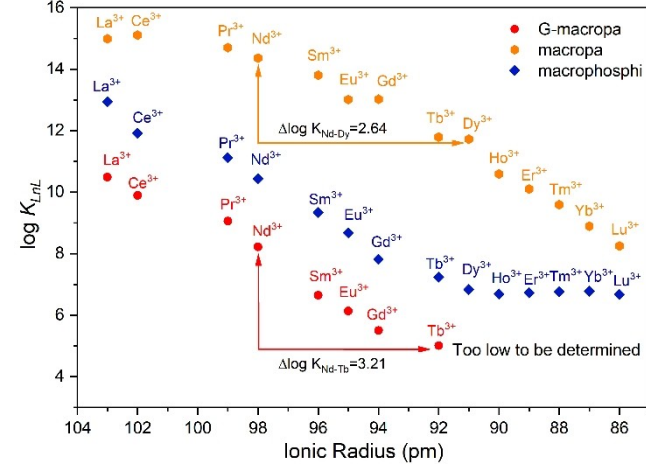


Figure 3. The Ln^{3+} stability constants (log K_{LnL}) of G-macropa, macropa, and macrophosphi versus ionic radii (CN = 6). Stability constants for G-macropa complexes of REEs heavier than Tb^{3+} are not included because they were too small to be reliably measured via this method.

macrocycle chelators. $^{[67,69,76]}$ In comparison to macropa and macrophosphi, however, the log $K_{\rm LnL}$ values for G-macropa are systematically smaller by 2–6 log units. Notably, G-macropa forms more stable complexes than bpa 18C6 by approximately 2 and 1 log units larger for log $K_{\rm LaL}$ and log $K_{\rm EuL}$, respectively. This higher affinity may be a consequence of outer-sphere electrostatic effects between the pendent glycine carboxylates and the ${\rm Ln}^{3+}$ ions.

Complex Structure Affects Ln³⁺—ligand Electrostatics and Stability

Molecular dynamics simulations were performed to optimize and compare the structures of the Nd³⁺ – and Dy³⁺ –macropa and G-macropa complexes in solution. From the complex structures for both geometries, electronic structure calculations were used to calculate binding energies and quantify the strength of the electrostatic interactions between different donor atoms on macropa and G-macropa with the Nd3+ and Dy3+ ions. The optimized Nd3+- and Dy3+-macropa complexes (Figure S29) have the picolinate donor arms coordinating the Ln3+ ion in a bidentate manner, along with two tertiary amine nitrogen atoms and four ether oxygen atoms from the macrocycle. Importantly, the optimized geometries are very similar to those observed experimentally via X-ray crystallography for macropa complexes of La³⁺ and smaller lanthanides.^[67,77] Also consistent with experimental observations, the optimized complexes of the larger Nd³⁺ contain a coordinated water molecule, but those of the smaller Dy3+ do not. The Ln3+-G-macropa complexes attained similar geometries, showing coordination via the neutral picolinamide donor arms.

With satisfactorily modeled structures of these complexes, the binding energies of these ligands for La³⁺, Nd³⁺, and Dy³⁺ (Eq. S1) were calculated and used to determine relative stability constants based on experimental data

(Eqs. S2-S4). These calculations reflect the reverse-size selectivity of macropa and its analogues, showing a larger binding affinity for Nd3+ compared to Dy3+. Significantly, there is a quantitative agreement between the predicted binding energies of the Nd3+ and Dy3+complexes of macropa and G-macropa relative to those of the corresponding La³⁺ complexes of the same ligand (Table 2). The relative free energies of binding, calculated from the stability constants with Eq. S2, are shown in Table 2 for both the experimental and computational data. The ratio of Nd³⁺ binding energies between the macropa and G-macropa ligands is predicted to be 0.49 by computation with Eq. S3 and Eq. S4, achieving a value that is very close to the ratio of 0.57 obtained via experimental stability constant measurements. Also noteworthy within these computational analyses is the fact that optimization of the Dy3+-G-macropa complex did not lead to a stable minimum (Table S2). This result is consistent with the experimental inability to quantify the stability constant of this complex due to the very weak nature of this interaction.

Having shown that the computational results agree favorably with experimental data, the origin of the differences in complex stability between the different REEs and chelators was investigated. An electrostatic potential (ESP) analysis of the coordination bonds within the Nd³⁺ and Dy³⁺ complexes of macropa and G-macropa was carried out using density functional theory (DFT) methods to understand the trends in the computed binding energies and measured stability constants with Eq. S5. Tables S3-S6 show the DFTcalculated electrostatic energy and the average interatomic distances for each coordination bond, the total electrostatic energy from all coordination bonds in each complex, as well as the ESP charges of the Ln³⁺ ion and coordinating atoms. The poorer stability of the Dy3+ complex of macropa compared to that of Nd3+ is reflected by different ESP charges on the Ln³⁺ center. The ESP charge on Dy³⁺ is 0.14 e, significantly smaller than the value of 0.45 e found on the Nd³⁺ center (Figure 4). The smaller ESP charge results in a lower electrostatic energy for the Dy³⁺ complex of macropa (Tables S3–S4), as observed experimentally. Furthermore, analysis of the G-macropa complex of Nd3+ reveals a smaller ESP on the Ln3+ of 0.16 e compared to the Ln3+ charge in the Nd3+-macropa complex (Table S5). These ESP charges are even smaller for the Dy3+ complex of Gmacropa (Table S6). Thus, the electron density in the Ln³⁺ ion within the Ln³⁺-ligand complex, quantified by the ESP

Table 2: Ln³+-macropa/La³+-macropa and Ln³+-G-macropa/La³+-G-macropa ratios calculated for experimental free energies of binding and computational binding energies using equations S3 and S4.

Complex	$(Ln/La)_{exp}$	$(Ln/La)_{comp}$
La ³⁺ —macropa	1 (reference)	1 (reference)
Nd ³⁺ -macropa	0.96	0.93
Dy ³⁺ -macropa	0.77	0.84
La ³⁺ —G-macropa	1 (reference)	1 (reference)
Nd ³⁺ –G-macropa	0.78	0.81
Dy ³⁺ —G-macropa	Undeterminable	Not binding

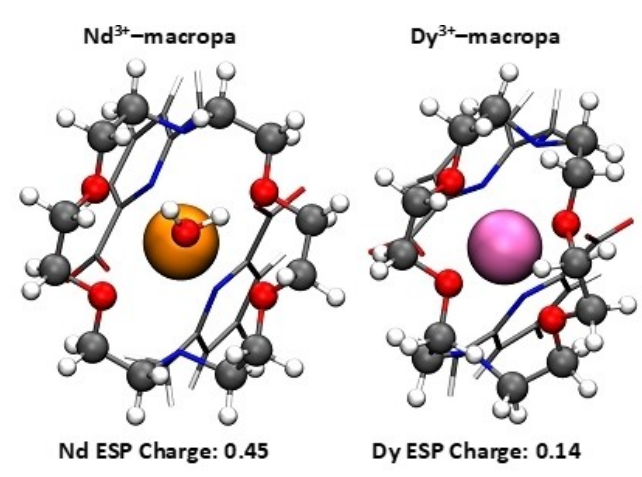


Figure 4. Left: In the ab initio molecular dynamics DFT-optimized Nd^{3+} —macropa complex, a coordinating water molecule expands the macrocyclic core, increasing the distances between the oxygen ether donors and the Ln^{3+} . Right: In the ab initio molecular dynamics DFT-optimized Dy^{3+} —macropa complex, the macrocycle contracts around the Dy^{3+} ion, due to the lack of coordinating water molecule. For clarity, the ball-and-stick representation is used for the macrocycle ethers with the rest of the ligand being represented as sticks. The Nd^{3+} ion is orange, Dy^{3+} ion is pink, nitrogen atoms are blue, oxygen atoms are red, carbon atoms are grey, and hydrogen atoms are white.

charge of the Ln³⁺ ion in the complex, correlates with the overall stability of the macropa and G-macropa complexes.

In understanding the difference between the Nd³⁺ and Dy³⁺ complexes of macropa, it is noteworthy that the Nd³⁺ complex of macropa accommodates an inner-sphere water molecule that is not found on the complex of the smaller Dy3+ ion. Without this inner-sphere water molecule, the macrocyclic core of the Dy3+ complex is substantially contracted (Figure 4), compared to that found in the Nd³⁺ complex. Consequently, the oxygen atoms within the macrocycle ether are arranged in an orientation that results in a smaller ESP charge of the Dy³⁺ ion, thereby decreasing the electrostatic energy of all the remaining coordination bonds within this complex. Similarly, in investigating the greater stability of Nd3+-macropa compared to Nd3+-G-macropa, the Nd³⁺ ion in the latter complex has a smaller ESP charge on the Nd³⁺ ion, leading to a decrease in electrostatic energy of all coordination bonds within this complex (Figure 5). Thus, the very weak binding of the Dy3+-G-macropa complex is a combination of both structural effects: the contraction of the macrocycle due to the lack of coordinated water, and picolinamide donors, results in a Dy³⁺ electron density with unfavorable electrostatic energies for binding.

Nd/Dy Separation Experiments

Based on the poor thermodynamic stability of G-macropa complexes for heavy REE, we reasoned that this chelator could selectively stabilize light REEs within solution, while allowing for heavy REEs to be selectively precipitated by HCO₃⁻ through the formation of insoluble Ln₂(CO₃)₃.^[78,79] This procedure would be particularly useful for the separa-

Nd ESP Charge: 0.45

Figure 5. Left: The ab initio molecular dynamics DFT-optimized Nd^{3+} —macropa complex showing the coordinating carboxylates of the picolinate donors in a ball-and-stick representation. Right: The ab initio molecular dynamics DFT-optimized Nd^{3+} —G-macropa complex with the coordinating glycine-amide functionalities of the picolinamide donors in a ball-and-stick representation. The same color scheme as that in Figure 4 is used.

Nd ESP Charge: 0.16

tion of light Nd^{3+} and heavy Dy^{3+} in electronic waste. Furthermore, $Dy_2(CO_3)_3$ is an important precursor for many technological applications of this element. In support of this separation strategy, the log K values follow the sequence of $[Nd(G\text{-macropa})]^+ > Dy_2(CO_3)_3 > Nd_2(CO_3)_3 > [Dy(G\text{-macropa})]^+$ (8.22, 6.10, 5.61, and <5, respectively), suggesting that a mixture of Nd^{3+} , Dy^{3+} , G-macropa, and HCO_3^- would favor the formation of soluble $[Nd(G\text{-macropa})]^+$ and insoluble $Dy_2(CO_3)_3$. As such, we explored the precipitation-based separation Scheme shown in Figure 6 at a low REE concentration of 500 μ M.

Following the separation procedure described in the Supporting Information and Figure 6, the separation efficiency (E, calculated by Eqs. S6 and S7) and REE distribution (calculated by Eqs. S8 and S9) were determined via inductively coupled plasma mass spectrometry (ICP-MS, Figure 7, Tables S7–S13). The pH of the solution initially after HCO_3^- addition and the final pH after filtration both remained close to 7. In absence of G-macropa, HCO_3^- (10 mM) precipitates both Nd^{3+} (250 μ M) and Dy^{3+} (250 μ M) from their 1:1 mixture with equal efficiency (~100%), consistent with the low and similar solubility product of their carbonates (pK_{sp} =33.98 and 34.10, respectively). [51] With varying amount of G-macropa, however, a significant difference, in precipitation efficiencies of these REEs are observed (Figure 7a). As the molar ratio of

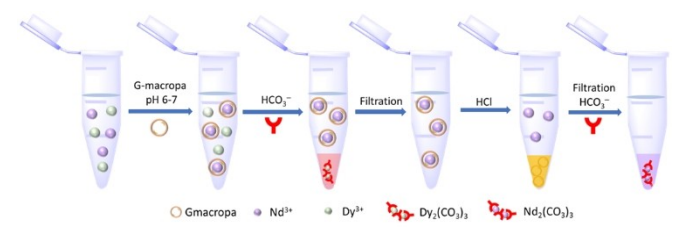


Figure 6. Depiction of the separation of a Nd^{3+}/Dy^{3+} mixture using G-macropa and HCO_3^- and the isolation of $Dy_2(CO_3)_3$, G-macropa, and $Nd_2(CO_3)_3$.

G-macropa to total Ln³+ (L/M ratio) is increased from 1 to 8, the percent quantity of the Nd³+ remaining in the filtrate also increased from 28.4 to 95.1 %. At the L/M ratio of 8, the filtrate is highly enriched in Nd³+ (97.4 %), leading the composition to be 96 % Dy³+ (Figure 7b), confirmed by energy-dispersive X-ray spectroscopy (EDS) analysis of these precipitates (Figure S30). Thus, the poor affinity of G-macropa for Dy³+ renders its precipitation with HCO₃⁻ to be highly efficient and selective. Its greater affinity with Nd³+, by contrast, favors formation of the water-soluble complex. In addition, this precipitation-based separation is fast. No changes in the elemental quantities within the filtrate nor precipitate occur after 1 h (Figure S31).

These results demonstrate how the selectivity of G-macropa for light REEs, like Nd³+, can facilitate their separation from heavy REEs, like Dy³+, via precipitation. The parent chelator macropa also exhibits a similar selectivity pattern as G-macropa. However, the use of this chelator, applied at L/M ratios ranging from 2–4, failed to yield any significant quantities of precipitate upon the addition of HCO₃⁻ (Figures 7c and 7d). The failure of HCO₃⁻ to induce precipitation of either REE in the presence of macropa is a consequence of the fact that this chelator has a substantially higher affinity for both REEs compared to G-macropa. Thus, the lower affinity afforded by G-macropa for the heavy REEs makes it useful for this type of REE separation.

These separation data can also be quantified via a SF. The SF parameter for precipitation-based separations is derived from distribution coefficients (D), the ratio of metal ions present within the solid and non-solid phases (Eqs. S10 and S11). The $SF_{\mathrm{Dy/Nd}}$ values increase as greater L/M ratios are applied. The largest $SF_{\rm Dy/Nd}$ is 841 for L/M=8 and $10\,\mathrm{mM}~\mathrm{HCO_3}^-$ (Figure 8). Based on the efficacy of the separation under these conditions, further studies using higher L/M ratios were not pursued. Further, the use of 8 equiv. of G-macropa with 1 mM HCO₃⁻ can also achieve excellent separation of Nd3+ and Dy3+ mixed at a molar ratio of 75:25. Under this optimized condition, Nd³⁺ is enriched to 96.8 % purity, and Dy³⁺ is upgraded from 25 % to 97%, leading to a very large $SF_{\rm Dy/Nd}$ of 741 (Table S10 and Figure S32). Table 3 shows a full comparison of our strategy and other novel chelators for the precipitation separation of Nd³⁺ and Dy³⁺. These very large SFs of 841 and 741 mark a significant advance in precipitation-based separations of these two elements, especially in the context of the fact that this process is operationally simple and is carried out in aqueous solution.

To further understand this separation process, we characterized the solution and solid-state products. ¹H NMR spectroscopy was carried out on the solutions before and after adding HCO₃⁻ to the mixture of Ln³⁺ and G-macropa at L/M=1. Without HCO₃⁻, the ¹H NMR spectrum shows only free G-macropa and [Nd(G-macropa)]⁺ in a 1:1 molar ratio, indicating that all Nd³⁺ ions are coordinated by G-macropa and the Dy³⁺ remains unbound (Figure S33). After adding HCO₃⁻, the ¹H NMR spectrum still presents the same species but in a ratio of 1.64:1. This observed loss of [Nd(G-macropa)]⁺ in the aqueous phase is a consequence of

5213773, 2024, 42, Downloaded from https://onlinelibrary.wiley.com/doi/10.1002/anie.202410233 by University Of Nevada Reno, Wiley Online Library on [1205/2025]. See the Terms and Conditions (https://onlinelibrary.wiley.com/terms-and-conditions) on Wiley Online Library for rules of use; OA articles are governed by the applicable Creative Commons License

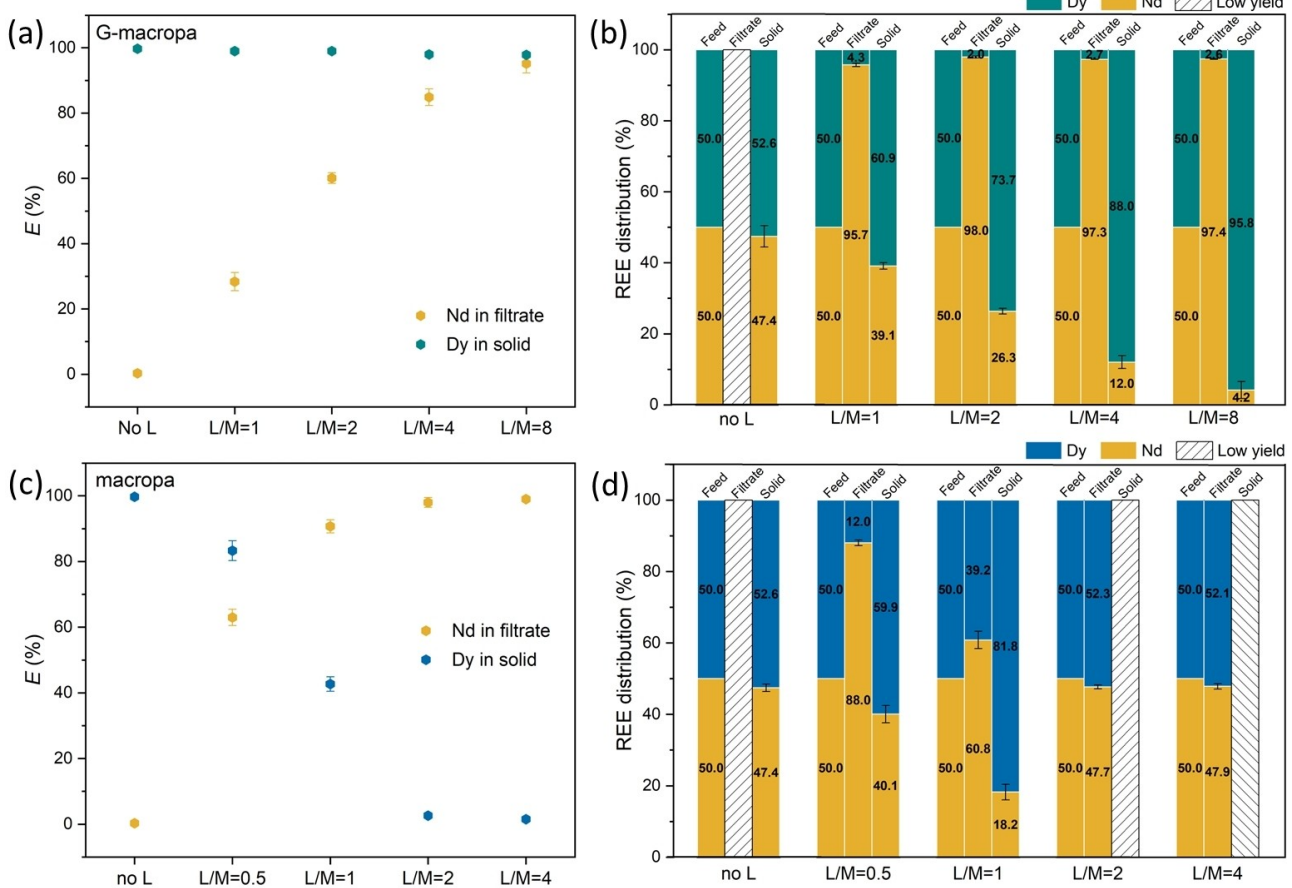


Figure 7. The separation efficiency of 1:1 Nd³⁺/Dy³⁺ mixture at different L/M ratios. (a) and (c) efficiency of Nd³⁺ maintained in filtrate and Dy³⁺ precipitated in the solid at different L/M ratios. (b) and (d) REE distribution percentage in filtrate and solid relative to the total metal in each phase. Conditions: $[Nd^{3+}] = 250 \,\mu\text{M}$, $[Dy^{3+}] = 250 \,\mu\text{M}$, $[L] = 0 - 4 \,\text{mM}$, $[HCO_3^-] = 10 \,\text{mM}$, $pH \sim 7$, $T = 22 \pm 1 \,^{\circ}\text{C}$. The error bars are reported as the standard deviation from two separations.

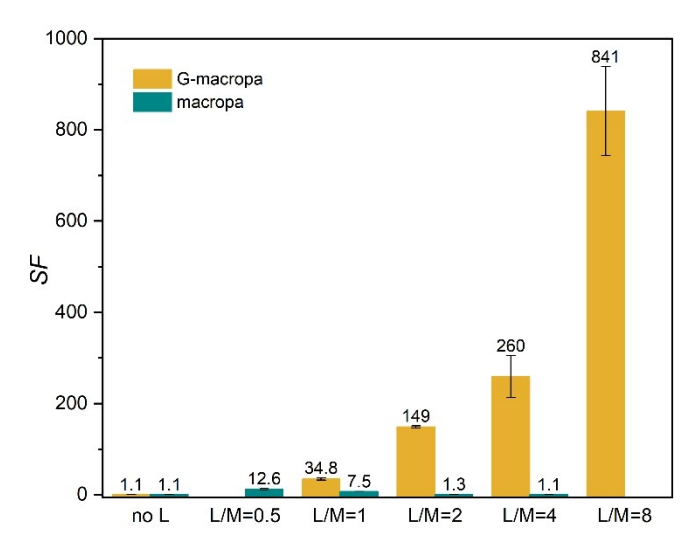


Figure 8. The SFs from G-macropa/HCO $_3^-$ precipitation of 250 μM Dy^{3+} and 250 $\mu M\ Nd^{3+}$ at different L/M ratios. L represents G-macropa (orange) or macropa (green). The error bars are reported as the standard deviation from two separations.

its partial incorporation into the solid Nd₂(CO₃)₃, as determined via ICP-MS for the L/M=1 experiment (Figure 7a). For the solid-phase characterization, X-ray photoelectron spectroscopy (XPS) and Fourier-transform infrared (FTIR) spectroscopy were employed. The XPS spectra of the precipitates obtained show sharp peaks from 3d and 4d orbitals of both Nd3+ and Dy3+ in the absence of Gmacropa. By contrast, in the presence of G-macropa, peaks arising from Dy3+ remain with the same intensity, but those of Nd³⁺ are no longer apparent (Figure S34a). Notably, the high-resolution XPS spectrum of the precipitate perfectly matches that of ACS grade Dy₂(CO₃)₃, displaying the doublets of Dy 3d and 4d valence electrons at 1334.8 eV/ 1297.6 eV and 156.6 eV/153.8 eV, respectively (Figures S34b and S34c). The FTIR spectrum of this solid also matches authentic Dy₂(CO₃)₃, displaying the characteristic peaks at 1493, 1403, and 835 cm⁻¹ from the vibrational modes of CO₃²⁻ (Figure S35).^[86,87] Additional low-intensity peaks at 1264 and 1121 cm⁻¹ were also present in this solid sample, and may arise from residual quantities of G-macropa. Thus, both the XPS and FTIR data indicate that highly pure Dy₂(CO₃)₃ solid can be isolated from these separations.

Research Article



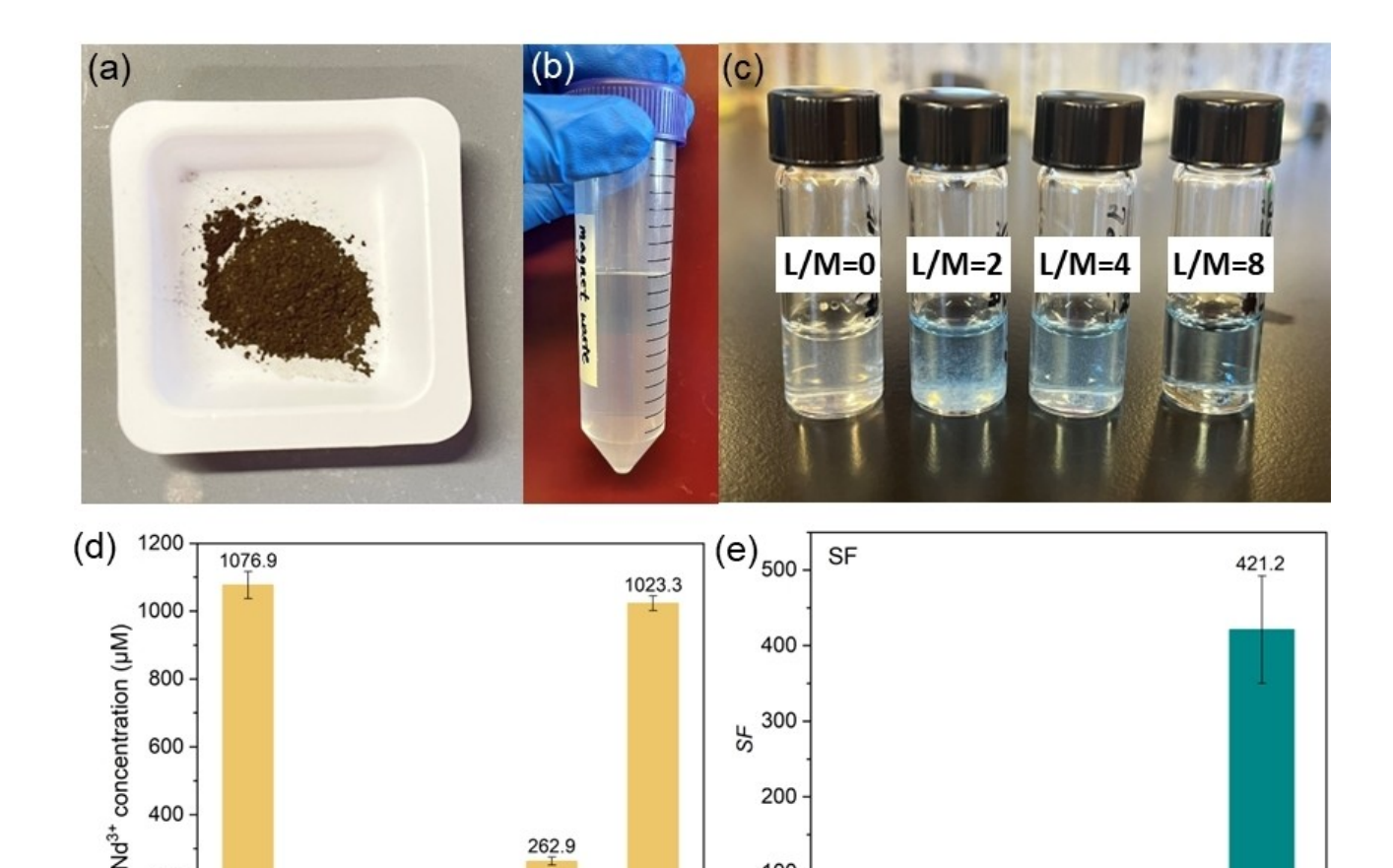
Table 3: Comparison of recent precipitation-based Nd/Dy separations.

Chelator (L)	Solvent	Product	SF	Total REE concentration	Ligand recovery yield/reagent	Reference
G-macropa/HCO ₃ ⁻	Water	Dy ₂ (CO ₃) ₃ /NdL	. 841–741 ^[a]	0.5 mM	76.5 %/HCl	This work
PQQ	Water	DyL/NdL	3.31	0.051 mM	n.r. ^[c] /HCl	[58]
Tripodal amido-arene	HNO ₃ /Toluene	Dy(NO) ₃ /NdL	Infinite ^[b]	2.5 mM	n.r. ^[c] /water	[59]
H ₃ TriNO ₂	THF/Benzene		359		87%(Nd ₂ L ₂) and 77%(DyL)/oxalic acid	[56]
H ₃ tren-1,2,3-HOPO·TFA	2.0 M HCl	DyL/NdCl ₃	213	39.5 mM	84%/HCl and EtOH	[82]
H ₃ TriNOx ^{OMe}	THF/Toluene	DyL/Nd ₂ L ₂	254	n.r. ^[c]	n.r. ^[c]	[83]
H ₃ TriNOx ^{OMe}	THF/Benzene	DyL/Nd ₂ L ₂	299	n.r. ^[c]	n.r. ^[c]	[83]
Trensalp-OMe	Acetone	DyL/NdL	7-10 ^[d]	7.74 mM	n.r. ^[c]	[84]
dibutylphosphoric acid (Hdbp)	Water	DyL/NdL	> 300	21 mM	n.r. ^[c]	[85]

[a] 841 for 50Nd/50Dy, 741 for 75Nd/25Dy. [b] Authors reported a SF of infinity based on the lack of observed Dy3+ precipitation. [c] n.r. = not reported. [d] SF calculated in this work from the authors' original data using Eqs. S10 and S11.

We next investigated this separation strategy in authentic Nd₂Fe₁₄B magnet waste containing Nd³⁺ and Dy³⁺ in a more challenging molar ratio of 95:5. This Nd₂Fe₁₄B magnet waste was acquired from a computer hard drive that was ground and separated into 30-mesh (0.595 mm) particle size

(Figure 9a). This powder was leached using 4 M HNO₃, a more oxidizing acid than HCl (Figure 9b),[88] and the metal ion concentrations within the resulting leachate were measured by ICP-MS (Table S11). As evident from these data, the magnet waste contains a wide range of different



L/M=8 Initial No L L/M=2 L/M=4 L/M=8 Figure 9. The efficiency of the G-macropa/HCO₃⁻ precipitation separation of Nd₂Fe₁₄B leachate for Nd³⁺ and Dy³⁺. (a) Photograph of the magnet waste powder used in this study. (b) The acidic leachate obtained after nitric acid digestion. (c) Magnet leachates after the G-macropa/HCO₃ separation. (d) The concentration of Nd^{3+} in the filtrate before and after G-macropa/ HCO_3^- precipitation. (e) The $SF_{Dy/Nd}$ from G-macropa/ $HCO_3^$ precipitation of magnet leachate at different L/M ratios. Conditions: [Nd³+] = 1077 μM, [Dy³+] = 48 μM, [L] = 0–8 mM, [HCO₃⁻] = 10 mM, pH ~7, $T=22\pm1$ °C. The error bars are reported as the standard deviation from two separations.

262.9

200

100

0

No L

400

200

0

40.8

L/M=4

12.8

L/M=2

5213773, 2024, 42, Downloaded from https://onlinelibrary.wiley.com/doi/10.1002/anie.202410233 by University Of Nevada Reno, Wiley Online Library on [1205/2025]. See the Terms and Conditions (https://onlinelibrary.wiley.com/terms-and-conditions) on Wiley Online Library for rules of use; OA articles are governed by the applicable Creative Commons License

metal ions from the s-, d-, and f-block. Within the f-block, the most highly abundant REE is Nd (3,132 μM), with substantially smaller quantities of Dy (141 µM) and Pr (13 µM). In addition to these REEs, Fe (21,192 µM), Al (12,686 µM), and Cu (4,474 µM) comprise the majority of other elements. Prior to Nd/Dy separation, > 99 % of the Fe was removed, along with smaller quantities of Al, Mg, and Cr, via an initial precipitation using saturated NaHCO₃(aq) to adjust the solution pH to 4 (Figure S36 and Table S11).^[89] After addition of G-macropa and a further pH increase to 7 with NaOH, more Al(OH)3 precipitated and was removed via filtration (Figure S37). With the majority of Fe and Al removed, the Nd/Dy separation was carried out via the addition of excess HCO₃⁻ at different L/M ratios of 2, 4, and 8 (Figure 9c). The metal concentration remaining in the filtrate after HCO₃⁻ addition was measured by ICP-MS. As shown in Figures 9d-9e and Table S12, with an increasing L/ M molar ratio, the amount of Nd3+ remaining in solution increases, while the Dy3+ present in the carbonate remains constant. A maximum Nd/Dy SF of 421 was achieved at L/M ratio of 8. These results demonstrate that our G-macropa/ HCO₃⁻ separation approach can be applied to complex

Lastly, we sought to demonstrate recyclability of this separation approach. Once the Dy₂(CO₃)₃ solid was isolated, the remaining aqueous solution from 8 independent separations was combined and concentrated via evaporation from 7.6 to ~2 mL. The addition of HCl triggered the recovery of the solid HCl salt of G-macropa (Figure 6 and Figure 10), which was confirmed by ¹H NMR spectroscopy (Figure S38) and elemental analysis. Notably, the ¹H NMR spectrum of the recovered solid displays peaks with identical chemicals shifts and multiplicities, as those found in authentic pure G-macropa samples (Figure S5). The recovered G-macropa yield of 76.5 % was calculated based on elemental analysis.

solutions that are directly relevant to electronic waste.

This yield could potentially be improved via further concentration of the filtrate. This recovered G-macropa was used for another separation of a 1:1 mixture of Nd^{3+}/Dy^{3+} , demonstrating no decrease in separation performance (Figure S39 and Table S13). In addition, after isolating G-macropa solid, the Nd^{3+} in acidic filtrate can be collected as solid $Nd_2(CO_3)_3$ in quantitative yield after the evaporation of solvent and the addition of saturated $NaHCO_3$. These results demonstrate the reusability of the G-macropa ligand, as well as the ability to obtain pure solid $Nd_2(CO_3)_3$.

The G-macropa/HCO₃⁻ system is advantageous in the perspective of environmental friendliness, high efficiency, and recyclability (Table 3). The use of water as the solvent, for example, marks an advantage over the seminal TriNOx³⁻, H₃TriNOx^{OMe}, tripodal amido-arene, and Trensalp-OMe separations of Nd³⁺ and Dy³⁺, which require THF, benzene, toluene, and acetone. [56,59,83,84] For the PQQ, H₃tren-1,2,3-HOPO, and Hdbp chelators, researchers were able to use water as a solvent, but the Nd/Dy *SF*s were substantially smaller than those obtained for G-macropa. [58,82,85] Moreover, the ability to recover G-macropa via simple acidification with a high yield indicates that this separation approach could become a cost-efficient new strategy to separate Nd/Dy on the industrial scale.

Conclusion

We have demonstrated an efficient, aqueous precipitationbased REE separation using G-macropa. In this separation strategy, we have leveraged the reverse-size selectivity of Gmacropa to complex Nd³⁺ in aqueous solution, which allows for the selective precipitation of Dy₂(CO₃)₃. This separation uses water as the only solvent and the common HCO₃⁻ anion as a precipitant, representing a significant advantage

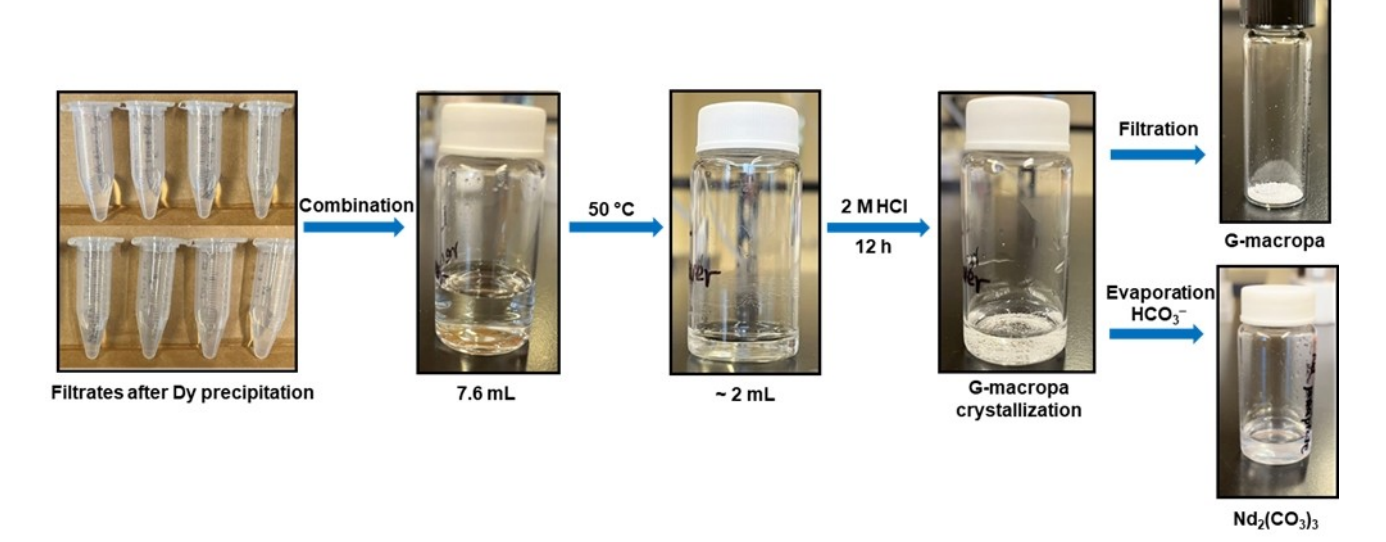


Figure 10. The procedure of G-macropa recovery. The filtrates from 8 separations were combined and concentrated to ~2 mL at 50 °C. HCl (1 mL, 6 M) was added to induce the crystallization of G-macropa as the HCl salt, while liberating Nd³⁺. The G-macropa HCl-salt was isolated by filtration. The Nd³⁺ in the acidic filtrate can be isolated as Nd₂(CO₃)₃ after the evaporation of the solvent followed by the addition of HCO₃⁻.



over conventional solvent extraction methods that require solvent and generate substantial quantities of waste. Furthermore, the ability to recover and reuse G-macropa for subsequent separations bodes well for the economic viability of this process. The implementation of operationally simple precipitation-based separations of the REEs is an increasing area of interest, as represented by a number of recent publications on this topic (Table 3). Further work will seek to apply this precipitation strategy with different chelators with distinct size-selectivity properties, [74,90,91] which may enable us to separate other types of REEs with similarly high efficiencies. Optimization of this approach for high concentration REE feedstocks is also needed. In this case, designing chelators with greater aqueous solubilities will enable their application in these high concentration solutions. In addition, the need for solvent concentration, an energy-intensive process, is a limitation of this system that requires further optimization. Lastly, life-cycle and technoeconomic analyses will help determine limitations of this approach that could be addressed in future design strategies to improve its large-scale viability. In particular, the cost of the synthesis and large-scale production of G-macropa would need to be addressed.

Supporting Information

The authors have cited additional references within the Supporting Information. [92-123]

Acknowledgements

This research is supported by USA Department of Energy Office of Science under award number DE-SC0021662. G. L. L. and D. C. C. acknowledge support from the National Science Foundation (Award 2041914). This research made use of the NMR Facility at Cornell University, which is supported, in part, by the NSF under Award CHE-1531632. Dr. Sean Medin (REEgen) is thanked for assistance with ICP-MS measurements. The hard drive magnet waste powder was provided by Dr. Erik Spiller and Dr. Brandon Ott at Colorado School of Mines by way of Dr. David Reed at Idaho National Lab.

Conflict of Interest

The authors declare no conflict of interest.

Data Availability Statement

The data that support the findings of this study are available in the supplementary material of this article.

Keywords: macrocyclic chelator · reverse-size selectivity · rare earth elements · precipitation separation

- [1] D. Bauer, D. Diamond, J. Li, D. Sandalow, P. Telleen, B. Wanner, "US Department of Energy Critical Materials Strategy", can be found under https://www.osti.gov/biblio/1000846, 2010 (accessed 2010–12–1).
- [2] V. Balaram, Geosci. Front. 2019, 10, 1285–1303.
- [3] J. A. Cotruvo, ACS Cent. Sci. 2019, 5, 1496-1506.
- [4] Z. Q. Bian, C. H. Huang, Rare Earth Coordination Chemistry: Fundamentals and Applications, VCH, Singapore, 2008.
- [5] W. M. Morrison, "CRS Report for Congress China's Rare Earth Industry and Export Regime: Economic and Trade Implications for the United States" can be found under https:// www.everycrsreport.com/reports/R42510.html, 2012. (accessed 2012–4–30).
- [6] A. Golevn, M. Scott, P. D. Erskine, S. H. Ali, G. R. Ballantyne, Resour. Policy 2014, 41, 52–59.
- [7] J. Bai, X. Xu, Y. Duan, G. Zhang, Z. Wang, L. Wang, C. Zheng, Sci. Rep. 2022, 12, 6105.
- [8] Y. El Ouardi, S. Virolainen, E. S. Massima Mouele, M. Laatikainen, E. Repo, K. Laatikainen, *Hydrometallurgy* 2023, 218, 106047.
- [9] J. Kujawa, S. Al Gharabli, A. Szymczyk, A. P. Terzyk, S. Boncel, K. Knozowska, G. Li, W. Kujawski, Coord. Chem. Rev. 2023, 493, 215340.
- [10] Y. Zhang, F. Gu, Z. Su, S. Liu, C. Anderson, T. Jiang, *Metals* 2020, 10, 841.
- [11] Y. Cao, P. Shao, Y. Chen, X. Zhou, L. Yang, H. Shi, K. Yu, X. Luo, X. Luo, Resour. Conserv. Recycl. 2021, 169, 105519.
- [12] Z. Chen, Z. Li, J. Chen, P. Kallem, F. Banat, H. Qiu, J. Environ. Chem. Eng. 2022, 10, 107104.
- [13] M. Firdaus, M. A. Rhamdhani, Y. Durandet, W. J. Rankin, K. McGregor, J. Sustain. Metall. 2016, 2, 276–295.
- [14] Z. Sun, H. Cao, Y. Xiao, J. Sietsma, W. Jin, H. Agterhuis, Y. Yang, ACS Sustainable Chem. Eng. 2017, 5, 21–40.
- [15] Q. Tan, J. Li, X. Zeng, Crit. Rev. Environ. Sci. Technol. 2015, 45, 749–776.
- [16] R. K. Jyothi, T. Thenepalli, J. W. Ahn, P. K. Parhi, K. W. Chung, J. Y. Lee, J. Cleaner Prod. 2020, 267, 122048.
- [17] S. Cotton, Lanthanide and Actinide Chemistry, John Wiley & Sons Ltd, Chichester, 2006.
- [18] R. B. Jordan, Inorg. Chem. 2023, 62, 3715-3721.
- [19] S. C. Bart, Inorg. Chem. 2023, 62, 3713–3714.
- [20] M. Seitz, A. G. Oliver, K. N. Raymond, J. Am. Chem. Soc. 2007, 129, 11153–11160.
- [21] K. N. Raymond, D. L. Wellman, C. Sgarlata, A. P. Hill, C. R. Chim. 2010, 13, 849–852.
- [22] N. A. Ismail, M. Aizudin, M. A. M. Aziz, M. Y. M. Yunus, A. Hisyam, *IJRTE*. 2019, 8, 728–743.
- [23] F. Xie, T. A. Zhang, D. Dreisinger, F. Doyle, *Miner. Eng.* 2014, 56, 10–28.
- [24] V. V. Belova, Theor. Found. Chem. Eng. 2017, 51, 599-609.
- [25] H. P. Neves, G. Max Dias Ferreira, G. Max Dias Ferreira, L. Rodrigues de Lemos, G. Dias Rodrigues, V. Albis Leão, A. Barbosa Mageste, Sep. Purif. Technol. 2022, 282, 120064.
- [26] P. A. Yudaev, N. A. Kolpinskaya, E. M. Chistyakov, *Hydro-metallurgy* 2021, 201, 105558.
- [27] D. Qi, Chapter 2 Extractants Used in Solvent Extraction-Separation of Rare Earths: Extraction Mechanism, Properties, and Features. In *Hydrometallurgy of Rare Earths: Extraction* and Separation, Elsevier Inc, 2018, pp.187–389.
- [28] K. R. Johnson, D. M. Driscoll, J. T. Damron, A. S. Ivanov, S. Jansone-Popova, *JACS Au* 2023, 3, 584–591.
- [29] D. R. Joshi, N. Adhikari, J. Pharm. Res. Int. 2019, 28, 49840.
- [30] P. Zapp, A. Schreiber, J. Marx, W. Kuckshinrichs, MRS Bull. 2022, 47, 267–275.
- [31] E. Vahidi, F. Zhao, J. Environ. Manage. 2017, 203, 255-263.

5213773, 2024



- [32] G. Dave, H. Blanck, K. Gustafsson, J. Chem. Technol. Biotechnol. 1979, 29, 249–257.
- [33] G. Dave, U. Lidman, Hydrometallurgy 1978, 3, 201–216.
- [34] G. K. Maiyoh, R. W. Njoroge, V. C. Tuei, Environ. Toxicol. Pharmacol. 2015, 40, 57–70.
- [35] N. N. Hidayah, S. Z. Abidin, Miner. Eng. 2017, 112, 103-113.
- [36] I. Anastopoulos, A. Bhatnagar, E. C. Lima, J. Mol. Liq. 2016, 221, 954–962.
- [37] X. Hérès, V. Blet, P. Di Natale, A. Ouaattou, H. Mazouz, D. Dhiba, F. Cuer, *Metals* 2018, 8, 682–699.
- [38] A. Ahmad, J. A. Siddique, M. A. Laskar, R. Kumar, S. H. Mohd-Setapar, A. Khatoon, R. A. Shiekh, J. Environ. Sci. 2015, 31, 104–123.
- [39] N. Kabay, J. L. Cortina, A. Trochimczuk, M. Streat, *React. Funct. Polym.* 2010, 70, 484–496.
- [40] G. S. Lee, M. Uchikoshi, K. Mimura, M. Isshiki, Sep. Purif. Technol. 2009, 67, 79–85.
- [41] Z. Dong, J. A. Mattocks, G. J-P. Deblonde, D. Hu, Y. Jiao, J. A. Cotruvo, D. M. Park, ACS Cent. Sci. 2021, 7, 1798–1808.
- [42] J. A. Mattocks, J. J. Jung, C.-Y. Lin, Z. Dong, N. H. Yennawar, E. R. Featherston, C. S. Kang-Yun, T. A. Hamilton, D. M. Park, A. K. Boal, J. A. Cotruvo, *Nature* 2023, 618, 87–93.
- [43] H. Cui, X. Zhang, J. Chen, X. Qian, Y. Zhong, C. Ma, H. Zhang, K. Liu, Adv. Mater. 2023, 35, 2303457.
- [44] Z. Dong, J. A. Mattocks, J. A. Seidel, J. A. Cotruvo, D. M. Park, Sep. Purif. Technol. 2024, 333,125919.
- [45] B. M. Jun, H. H. Kim, H. Rho, J. Seo, J. W. Jeon, S. N. Nam, C. Min Park, Y. Yoon, *Chem. Eng. J.* 2023, 475, 146222.
- [46] B. Hu, M. He, B. Chen, Z. Jiang, Phys. Sci. Rev. 2016, 1, 20160056.
- [47] R. F. Higgins, K. P. Ruoff, A. Kumar, E. J. Schelter, Acc. Chem. Res. 2022, 55, 2616–2627.
- [48] Q. Wang, C. V. Subban, RSC Sustain. 2024, 2, 1400–1407.
- [49] T. V. Hoogerstraete, B. Blanpain, T. Van Gerven, K. Binnemans, RSC Adv. 2014, 4, 64099–64111.
- [50] A. L. Sarver, P. M-P Brinton, J. Am. Chem. Soc. 1927, 49, 943-958.
- [51] F. Henry Flrschlng, J. Mohammadzadel, J. Chem. Eng. Data 1986, 31, 40–42.
- [52] P. Kim, A. Anderko, A. Navrotsky, R. E. Riman, *Minerals* 2018, 8, 106.
- [53] B. E. Cole, T. Cheisson, J. J. M. Nelson, R. F. Higgins, M. R. Gau, P. J. Carroll, E. J. Schelter, ACS Sustainable Chem. Eng. 2020, 8, 14786–14794.
- [54] J. A. Bogart, B. E. Cole, M. A. Boreen, C. A. Lippincott, B. C. Manor, P. J. Carroll, E. J. Schelter, *Proc. Natl. Acad. Sci. USA* 2016, 113, 14887–14892.
- [55] D. N. Mangel, G. J. Juarez, S. H. Carpenter, A. Steinbrueck, V. M. Lynch, J. Yang, A. C. Sedgwick, A. Tondreau, J. L. Sessler, J. Am. Chem. Soc. 2023, 145, 22206–22212.
- [56] J. A. Bogart, C. A. Lippincott, P. J. Carroll, E. J. Schelter, Angew. Chem. Int. Ed. 2015, 127, 8340–8343.
- [57] R. F. Higgins, T. Cheisson, B. E. Cole, B. C. Manor, P. J. Carroll, E. J. Schelter, *Angew. Chem. Int. Ed.* 2020, 132, 1867– 1872
- [58] H. Lumpe, A. Menke, C. Haisch, P. Mayer, A. Kabelitz, K. V. Yusenko, A. G. Buzanich, T. Block, R. Pöttgen, F. Emmerling, L. J. Daumann, *Chem. Eur. J.* 2020, 26, 10133–10139.
- [59] J. G. O'Connell-Danes, B. T. Ngwenya, C. A. Morrison, J. B. Love, Nat. Commun. 2022, 13, 4497.
- [60] H. Yang, F. Peng, D. E. Schier, S. A. Markotic, X. Zhao, A. N. Hong, Y. Wang, P. Feng, X. Bu, *Angew. Chem. Int. Ed.* 2021, 60, 11148–11152.
- [61] P. Yang, Q. Zhuang, Y. Li, J. Gu, Chem. Commun. 2019, 55, 14902–14905.

- [62] H. Lu, X. Guo, Y. Wang, K. Diefenbach, L. Chen, J. Q. Wang, J. Lin, S. Wang, *Dalton Trans.* 2019, 48, 12808–12811.
- [63] H. Y. Gao, W. L. Peng, P. P. Meng, X. F. Feng, J. Q. Li, H. Q. Wu, C. S. Yan, Y. Y. Xiong, F. Luo, *Chem. Commun.* 2017, 53, 5737–5739.
- [64] Z. Bai, B. Scheibe, J. M. Sperling, T. E. Albrecht-Schönzart, Inorg. Chem. 2022, 61, 19193–19202.
- [65] X. Yin, Y. Wang, X. Bai, Y. Wang, L. Chen, C. Xiao, J. Diwu, S. Du, Z. Chai, T. E. Albrecht-Schmitt, S. Wang, *Nat. Commun.* 2017, 8, 14438.
- [66] A. Hu, J. J. Wilson, Acc. Chem. Res. 2022, 55, 904-915.
- [67] A. Roca-Sabio, M. Mato-Iglesias, D. Esteban-Gómez, É. Toth, A. De Bias, C. Platas-Iglesias, T. Rodríguez-Blas, J. Am. Chem. Soc. 2009, 131, 3331–3341.
- [68] N. A. Thiele, J. J. Woods, J. J. Wilson, *Inorg. Chem.* 2019, 58, 10483–10500.
- [69] N. A. Thiele, D. Fiszbein, J. J. Woods, J. J. Wilson, *Inorg. Chem.* 2020, 59, 16522–16530.
- [70] K. J. Kadassery, A. P. King, S. Fayn, K. E. Baidoo, S. N. MacMillan, F. E. Escorcia, J. J. Wilson, *Bioconjugate Chem.* 2022, 33, 1222–1231.
- [71] M. P. Jensen, R. Chiarizia, I. A. Shkrob, J. S. Ulicki, B. D. Spindler, D. J. Murphy, M. Hossain, A. Roca-Sabio, C. Platas-Iglesias, A. De Blas, T. Rodríguez-Blas, *Inorg. Chem.* 2014, 53, 6003–6012.
- [72] Z. Baranyai, E. Brücher, T. Iványi, R. Király, I. Lázár, L. Zékány, Helv. Chim. Acta 2005, 88, 604–617.
- [73] A. Pasha, G. Tircsó, E. T. Benyó, E. Brücher, A. D. Sherry, Eur. J. Inorg. Chem. 2007, 2007, 4340–4349.
- [74] A. Hu, S. N. MacMillan, J. J. Wilson, J. Am. Chem. Soc. 2020, 142, 13500–13506.
- [75] M. Regueiro-Figueroa, J. L. Barriada, A. Pallier, D. Esteban-Gómez, A. De Blas, T. Rodríguez-Blas, É. Tóth, C. Platas-Iglesias, *Inorg. Chem.* 2015, 54, 4940–4952.
- [76] N. A. Thiele, J. J. Woods, J. J. Wilson, *Inorg. Chem.* 2019, 58, 10483–10500.
- [77] N. A. Thiele, V. Brown, J. M. Kelly, A. Amor-Coarasa, U. Jermilova, S. N. MacMillan, A. Nikolopoulou, S. Ponnala, C. F. Ramogida, A. K. H. Robertson, C. Rodríguez-Rodríguez, P. Schaffer, C. Williams, J. W. Babich, V. Radchenko, J. J. Wilson, *Angew. Chem. Int. Ed.* 2017, 56, 14712–14717.
- [78] N. Yanagihara, K. Vemulapalli, Q. Fernando, J. T. Dyke, J. Less-Common Met. 1991, 167, 223–232.
- [79] R. Janicki, P. Starynowicz, A. Mondry, Eur. J. Inorg. Chem. 2011, 2011, 3601–3616.
- [80] Heegermaterials, "Dysprosium Carbonate Tetrahydrate Powder," can be found under https://heegermaterials.com/dysprosium/875-dysprosium-carbonate.html, 2013 (accessed 2013–3– 1).
- [81] K. J. Cantrell, R. H. Byrne, Geochim. Cosmochim. Acta 1987, 51, 597–605.
- [82] J. J. M. Nelson, T. Cheisson, H. J. Rugh, M. R. Gau, P. J. Carroll, E. J. Schelter, *Commun. Chem.* 2020, 3, 7.
- [83] B. E. Cole, I. B. Falcones, T. Cheisson, B. C. Manor, P. J. Carroll, E. J. Schelter, *Chem. Commun.* 2018, 54, 10276– 10279.
- [84] A. Falco, M. Neri, M. Melegari, L. Baraldi, G. Bonfant, M. Tegoni, A. Serpe, L. Marchiò, *Inorg. Chem.* 2022, 61, 16110–16121.
- [85] Y. Tasaki-Handa, Y. Abe, K. Ooi, H. Narita, M. Tanaka, A. Wakisaka, J. Phys. Chem. B 2016, 120, 12730–12735.
- [86] B. Vallina, J. D. Rodriguez-Blanco, A. P. Brown, J. A. Blanco, L. G. Benning, J. Nanopart. Res. 2013, 15, 1438.
- [87] M. Rahimi-Nasrabadi, S. M. Pourmortazavi, M. R. Ganjali, P. Novrouzi, F. Faridbod, M. S. Karimi, J. Mater. Sci.: Mater. Electron. 2017, 28, 3325–3336.

5213773, 2024

, 42, Downloaded from https://onlinelibrary.wiley.com/doi/10.1002/anie.202410233 by University Of Nevada Reno, Wiley Online Library on [1205/2023]. Sethe Terms and Conditions (https://onlinelibrary.wiley.com/terms-and-conditions) on Wiley Online Library for rules of use; OA articles are governed by the applicable Creative Commons License

- [88] M. Gergoric, C. Ekberg, M. R. S. J. Foreman, B. M. Steenari, T. Retegan, J. Sustain. Metall. 2017, 3, 638–645.
- [89] Y. Wu, S. Zhang, G. Wang, T. Li, X. Xu, Y. Pu, W. Zhou, Y. Li, Y. Jia, J. Cleaner Prod. 2023, 423, 138782.
- [90] A. Hu, E. Aluicio-Sarduy, V. Brown, S. N. MacMillan, K. V. Becker, T. E. Barnhart, V. Radchenko, C. F. Ramogida, J. W. Engle, J. J. Wilson, J. Am. Chem. Soc. 2021, 143, 10429–10440.
- [91] A. Hu, M. E. Simms, V. Kertesz, J. J. Wilson, N. A. Thiele, *Inorg. Chem.* 2022, 61, 12847–12855.
- [92] CrysAlisPro; Rigaku OD, The Woodlands, TX, 2015.
- [93] G. M. Sheldrick, Acta Crystallogr. Sect. 2015, 71, 3-8.
- [94] G. M. Sheldrick, Acta Crystallogr. Sect. A 2008, 64, 112-122.
- [95] P. Müller, Crystallogr. Rev. 2009, 15, 57-83.
- [96] F. H. Sweeton, R. E. Mesmer, C. F. Baes, J. Solution Chem. 1974, 3, 191–213.
- [97] G. Gran, Acta Chem. Scand. 1950, 4, 559-577.
- [98] G. Gran, Analyst 1948, 73, 561a-561a.
- [99] P. Gans, B. O'Sullivan, Talanta 2000, 51, 33-37.
- [100] T. Song, P. Cheng, X. Wang, J. Xu, Analytical Chemistry I, 5th Ed.; Higher Education Press: Beijing, 2006.
- [101] P. Gans, A. Sabatini, A. Vacca, Talanta 1996, 43, 1739-1753.
- [102] W. L. Jorgensen, D. S. Maxwell, J. Tirado-Rives, J. Am. Chem. Soc. 1996, 118, 11225–11236.
- [103] M. J. Abraham, T. Murtola, R. Schulz, S. Páll, J. C. Smith, B. Hess, E. Lindah, *SoftwareX* 2015, 1–2, 19–25.
- [104] T. D. Kühne, M. Iannuzzi, M. Del Ben, V. V. Rybkin, P. Seewald, F. Stein, T. Laino, R. Z. Khaliullin, O. Schütt, F. Schiffmann, D. Golze, J. Wilhelm, S. Chulkov, M. H. Bani-Hashemian, V. Weber, U. Borštnik, M. Taillefumier, A. S. Jakobovits, A. Lazzaro, H. Pabst, T. Müller, R. Schade, M. Guidon, S. Andermatt, N. Holmberg, G. K. Schenter, A. Hehn, A. Bussy, F. Belleflamme, G. Tabacchi, A. Glöß, M. Lass, I. Bethune, C. J. Mundy, C. Plessl, M. Watkins, J. VandeVondele, M. Krack, J. Hutter, J. Chem. Phys. 2020, 152, 194103.
- [105] J. VandeVondele, M. Krack, F. Mohamed, M. Parrinello, T. Chassaing, J. Hutter, Comput. Phys. Commun. 2005, 167, 103–128.
- [106] J. P. Perdew, K. Burke, M. Ernzerhof, Phys. Rev. Lett. 1996, 77, 3865–3868.

- [107] J. B. Lu, D. C. Cantu, M. T. Nguyen, J. Li, V. A. Glezakou, R. Rousseau, J. Chem. Theory Comput. 2019, 15, 5987–5997.
- [108] J. VandeVondele, J. Hutter, J. Chem. Phys. **2007**, 127, 114105.
- [109] S. Grimme, J. Antony, S. Ehrlich, H. Krieg, J. Chem. Phys. 2010, 132, 154104.
- [110] V. Barone, M. Cossi, J. Phys. Chem. A 1998, 102, 1995–2001.
- [111] F. Neese, F. Wennmohs, D. Aravena, M. Atanasov, U. Becker, G. Bistoni, D. Bykov, V. G. Chilkuri, D. Datta, A. K. Dutta, D. Ganyushin, M. Garcia, Y. Guo, A. Hansen, B. Helmich-Paris, L. Huntington, R. Izsák, C. Kollmar, S. Kossmann, M. Krupička, L. Lang, D. Lenk, D. G. Liakos, D. Manganas, D. A. Pantazis, T. Petrenko, P. Pinski, C. Reimann, M. Retegan, C. Riplinger, T. Risthaus, M. Roemelt, M. Saitow, B. Sandhöfer, I. Schapiro, K. Sivalingam, B. De Souza, G. Stoychev, W. Van Den Heuvel, B. Wezisla, M. Kállay, S. Grimme, E. Valeev, G. Chan, J. Pittner, M. Brehm, L. Goerigk, V. Vilhjálmuråsgeirsson, W. Schneider, ORCA—An Ab Initio, DFT and Semiempirical SCF-MO Package-Version 4.2.1.
- [112] F. Neese, WIREs Comput. Mol. Sci. 2022, 12, e1606.
- [113] Y. Zhao, D. G. Truhlar, Theor. Chem. Acc. 2008, 120, 215– 241
- [114] M. Douglas, N. M. Kroll, Ann. Phys. 1974, 82, 89–155.
- [115] B. A. Hess, Phys. Rev. A 1985, 32, 756-763.
- [116] D. A. Pantazis, X. Y. Chen, C. R. Landis, F. Neese, J. Chem. Theory Comput. 2008, 4, 908–919.
- [117] D. E. Woon, T. H. Dunning, J. Chem. Phys. 1995, 103, 4572– 4585.
- [118] J. Zheng, X. Xu, D. G. Truhlar, Theor. Chem. Acc. 2011, 128, 295–305.
- [119] C. M. Breneman, K. B. Wiberg, J. Comput. Chem. 1990, 11, 361–373.
- [120] S. R. Cox, D. E. Williams, J. Comput. Chem. 1981, 2, 304–323.
- [121] X. Cao, M. Dolg, J. Mol. Struct. 2002, 581, 139-147.
- [122] X. Cao, M. Dolg, J. Chem. Phys. 2001, 115, 7348–7355.
- [123] T. H. Dunning, J. Chem. Phys. 1989, 90, 1007–1023.

Manuscript received: May 30, 2024 Accepted manuscript online: July 18, 2024 Version of record online: September 6, 2024